ELSEVIER

Journal of Nuclear Materials 302 (2002) 185–192

journal of nuclear materials

www.elsevier.com/locate/jnucmat

On irradiation embrittlement and recovery annealing mechanisms of Cr–Mo–V type pressure vessel steels

Risto Ilola [a,*], Vladimir Nadutov [b], Matti Valo [c], Hannu Hänninen [a]

[a] *Helsinki University of Technology, Laboratory of Engineering Materials, P.O. Box 4200, FIN-02015 HUT, Finland*
[b] *G.V. Kurdyumov Institute of Metal Physics of the Academy of Sciences of Ukraine, 36 Vernadsky Blvd, 252680 Kiev-142, Ukraine*
[c] *VTT Industrial Systems, P.O. Box 17042, FIN-02044 VTT, Finland*

Received 5 November 2001; accepted 17 January 2002

Abstract

Surveillance specimens of 15Kh2MFA reactor pressure vessel (RPV) steel and Sv-10KhMFT weld metal were investigated using internal friction, electrical resistivity and Mössbauer spectroscopy measurements in order to obtain information on their irradiation embrittlement and recovery annealing mechanisms. Internal friction measurements showed that carbon becomes trapped by irradiation-induced defects (fluence $= 4.1 \times 10^{19}$ n/cm^2, $E > 1$ MeV, $T = 265$ °C). During the recovery annealing (450 and 475 °C/1 h) carbon does not redissolve into the solid solution. Although irradiation usually increases the electrical resistivity of the RPV steels, in this study irradiation decreased the electrical resistivity of both the base and the weld metals. This can be due to a decrease in the dislocation density or precipitation under irradiation. The annealing temperature range for recovery was 300–600 °C for the base and the weld metals according to the electrical resistivity measurements. Some evidence of irradiation-induced carbide formation was achieved by the Mössbauer spectroscopy measurements.

1. Introduction

Irradiation embrittlement is one of the major degradation mechanisms of ferritic reactor pressure vessel (RPV) steels [1–4]. It is caused by fast neutron ($E > 1$ MeV) collisions to the RPV wall creating defects and defect clusters which restrict the movement of glide dislocations. The point defects (interstitials and vacancies) created in the displacement cascades during neutron irradiation can recombine, become trapped by impurity atoms, cluster and collapse to dislocation loops (interstitial), coalesce, and form nano-voids or migrate to defect sinks such as interfaces and dislocations. Irradiation increases the diffusion rate by increasing the vacancy concentration, which enhances precipitation and/or clustering of the alloying elements. Recently, attention has been paid, not only to Cu- and P-rich precipitates, but also to carbides. On the macroscopic level, neutron irradiation results in deterioration of mechanical properties and ductility of the ferritic RPV steels, i.e., increase in the ductile-to-brittle transition temperature and decrease in the upper self-impact energy as well as increase in the yield strength and decrease in the strain hardening capacity [2–4].

Thermal annealing of embrittled RPV steels restores their mechanical properties [1,3,4]. The phenomenon is known as recovery annealing, but the microscopic mechanisms of recovery have remained unclear. Understanding the micromechanisms concerning irradiation embrittlement and recovery annealing (and also reembrittlement due to irradiation) behaviour would validate the experimentally determined annealing parameters (time and temperature) and considerably contribute to the safety assessment of the recovery annealed RPVs.

The base metal of the VVER-440 type reactors is 15Kh2MFA steel (Cr–Mo–V steel). The weld metal used

* Corresponding author. Tel.: +31-224 565 251; fax: +31-224 563 125.
E-mail addresses: ilola@jrc.nl, risto.ilola@hut.fi (R. Ilola).

0022-3115/02/$ - see front matter
PII: S0022-3115(02)00780-8

in the circumferential submerged arc welds is Sv-10KhMFT. The microstructure of the base metal resulting from the heat treatment during the manufacturing process (austenization at 1000 °C with oil quenching, followed by tempering at approximately 700 °C) consists of tempered bainite with a rather complicated carbide structure [5–7]. The carbide structure consists of MC, M_7C_3 and $M_{23}C_6$ carbides. The carbide precipitation begins at 450 °C as vanadium-rich carbides (MC). Simultaneously, or at somewhat higher temperatures iron–chromium carbides (M_3C) precipitate. These are replaced by M_7C_3 carbides at higher temperatures. M_7C_3 can alternatively be Fe_2MoC. $M_{23}C_6$ (chromium-rich) carbides are found at higher temperatures [7]. According to [7], dislocation densities of the order of 5×10^{14} l/m^2 can be expected in the base metal after the performed heat treatment. The microstructure of the weld metal resulting from the heat treatment (annealing at 620–660 °C for ≈50 h) consists of chromium-rich carbides on the grain boundaries and VC plates within the grains [6].

The aim of this study was to test the suitability of internal friction, electrical resistivity and Mössbauer spectroscopy measurements to investigate irradiation embrittlement and recovery annealing mechanisms and the irradiation-induced structures in the base and the weld metals used in the VVER-440 type pressurized water reactors.

2. Experimental methods

The test materials used were a 15Kh2MFA RPV steel (base metal) and a Sv-10KhMFT submerged arc weld metal. The test materials were studied in the unirradiated and irradiated conditions. The chemical compositions of the test materials are given in Table 1. For the base metal, the heat treatment was austenization at 1000 °C (12 h) with an oil quench, followed by double tempering: first at 700 °C (25 h) and second at 670 °C (40 h). The submerged arc welds were heat treated for approximately 50 h at 620–660 °C. The test materials were irradiated in the surveillance positions of the Loviisa nuclear power plant up to a fluence of 4.1×10^{19} n/cm^2 ($E > 1$ MeV) at 265 °C.

Internal friction measurements were performed in an inverted pendulum apparatus [8]. The samples were first cut to a size of $0.8 \times 0.8 \times 27$ mm^3 and then etched to their final size ($0.6 \times 0.6 \times 27$ mm^3) using a hydrofluoric acid and hydrogen peroxide solution (4% HF + 96% H_2O_2). The measurements were performed in 20 Pa helium atmosphere in a frequency range of 0.5–0.6 Hz. The strain amplitude and the heating rate during the measurements were 3×10^{-6} and 0.03 °C/s, respectively. Internal friction was measured as a function of temperature in the temperature range of −196 to 230 °C. A saturating magnetic field was used during measurements in order to eliminate the effects of the magnetic domain wall movements on internal friction results.

Electrical resistivity was measured using an automatic four point AC-resistivity bridge (AVS-100 by Picowatt, Vantaa, Finland). Electrical resistivity was measured at liquid helium (−269 °C) and liquid nitrogen (−196 °C) temperatures and at room temperature (25 °C). The 'zig-zag' specimens were cut from $10 \times 10 \times 0.3$ mm^3 pieces. After cutting they were etched using a hydrofluoric acid and hydrogen peroxide solution (4% HF + 96% H_2O_2). The nominal cross-section area/length ratio of the specimens was 8.6×10^{-5} cm. Copper leads were spot welded at the ends of the specimens. The specimens were isocronally annealed in a tube furnace in an argon atmosphere for 0.5 h in steps of 50 °C in the temperature range of 250–650 °C. The argon atmosphere was used to avoid decarburization and oxidation during the annealing. Specific resistivity of the test materials was determined using the nominal cross-section area/length ratio.

Mössbauer measurements were performed in the transmission geometry using a Halder spectrometer and a NP-255 spectrometer where ^{57}Co in a Cr matrix was used as the source of gamma quanta. The specimens were etched in a hydrofluoric acid and hydrogen peroxide solution (4% HF + 96% H_2O_2) to their final thickness of about 20 μm. The cross-section area of the specimens was approximately 1 cm^2.

Table 1
Chemical compositions of the test materials

Material	Composition (wt%)										
	C	Si	Mn	S	P	Cu	Cr	Ni	Mo	V	Co
Base metal (15Kh2MFA)	0.16	0.27	0.39	0.012	0.010	0.10	2.5	0.19	0.63	0.29	0.01
Weld metal (Sv-10KhMFT)	0.04	0.62	1.05	0.022	0.019	0.22	1.6	0.16	0.46	0.21	0.02

3. Results

3.1. Internal friction

Internal friction Snoek peak measurements were used to observe changes in the free carbon content in the matrix of 15Kh2MFA steel. The Snoek peak arises from the transition of carbon atoms between neighbouring interstitial sites and it is proportional to the carbon content in a solid solution [9].

Irradiation clearly affects the Snoek peak height, which was observed in the preliminary test measurements performed with a 0.18 wt% carbon containing structural steel (Fig. 1). Internal friction results for 15Kh2MFA steel are shown in Fig. 2. A small peak appeared in the unirradiated state at 57 °C. According to the location of the peak it is related with Snoek relaxation. The peak is assumed to be only due to carbon atoms because all nitrogen should be in nitrides after the heat treatment of the base metal. In addition to this, the nitrogen Snoek peak appears at lower temperatures than the carbon Snoek peak [9]. The internal friction peak disappeared after irradiation of the base metal to a fluence of 4.1×10^{19} n/cm^2, $E > 1$ MeV. After post-irradiation heat treatments at recovery annealing temperatures of 450 and 475 °C for 1 h, the Snoek peak did not reappear. No changes in the internal friction spectra were observed at temperatures below 0 °C and between 120 and 230 °C, which was the maximum operating temperature of the apparatus used. Different internal friction background values in Fig. 2 are due to the specimen mounting and they have no effect on the results. Internal friction was not measured for the weld metal because of the relatively small Snoek peak in the base metal.

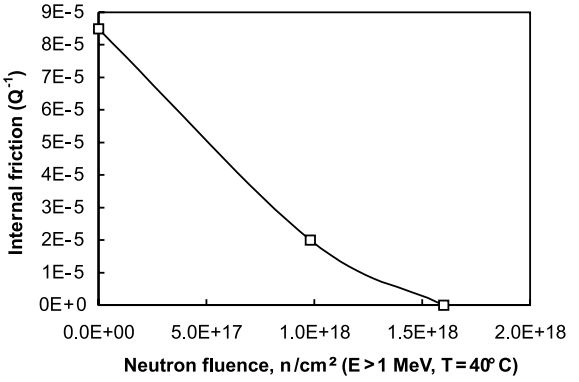

Fig. 1. Decrease in the internal friction peak height as a function of neutron fluence for 0.18 wt% structural steel. Heat treatment before irradiation: normalization 915 °C/1 h, air cooling, tempering 150 °C/5 h, sample size: $0.7 \times 0.7 \times 45$ mm^3, strain amplitude: 3×10^{-6}, heating rate: 1.2 °C/min.

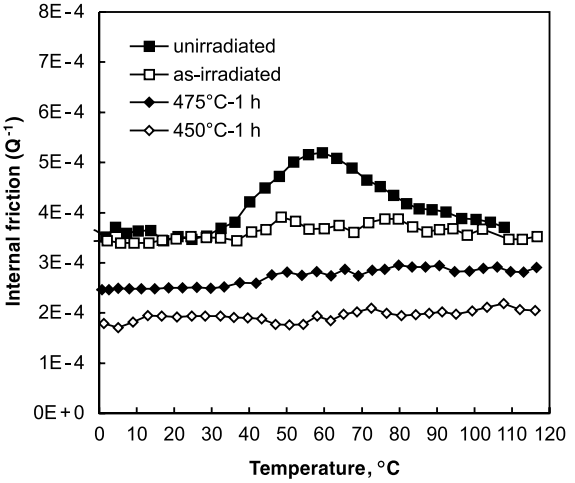

Fig. 2. Results of the internal friction measurements for 15Kh2MFA steel. Sample size: $0.6 \times 0.6 \times 27$ mm^3, strain amplitude: 3×10^{-6} and heating rate: 2 °C/min. Studied samples: unirradiated, irradiated (4.1×10^{19} n/cm^2 at 265 °C, $E > 1$ MeV), irradiated and annealed (450 °C/1 h, Ar) and irradiated and annealed (475 °C/1 h, Ar).

3.2. Electrical resistivity

The results of the electrical resistivity measurements at liquid helium temperature (−269 °C) after annealing at different temperatures are presented in Fig. 3. Surprisingly, in both the base and the weld metals the resistivity was lower in the irradiated (4.1×10^{19} n/cm^2, $E > 1$ MeV) than in the unirradiated state. After thermal annealing the resistivity increased in all specimens. The increase was greatest in the irradiated weld metal starting at 300 °C. The main increase was observed between 400–550 °C after which it saturated at about 600 °C. The shapes of the resistivity curves were not changed when the measurements were performed at liquid nitrogen temperature (−196 °C), but a uniform increase of the specific resistivity was approximately 1.5 μΩcm. A similar change was not observed in the room temperature measurements due to an increasing effect of phonons.

The higher electrical resistivity values of the weld metals as compared with those of the base metals result from a larger number of defects in the crystal lattice and a larger alloying element content (e.g. Si, Mn, S and Cu) in the weld metal.

3.3. Mössbauer spectroscopy

Typical Mössbauer spectra of 15Kh2MFA RPV steel are presented in Fig. 4. The spectrum of the unirradiated base metal can be decomposed into six components with hyperfine parameters (Table 2). Components 2 and 3,

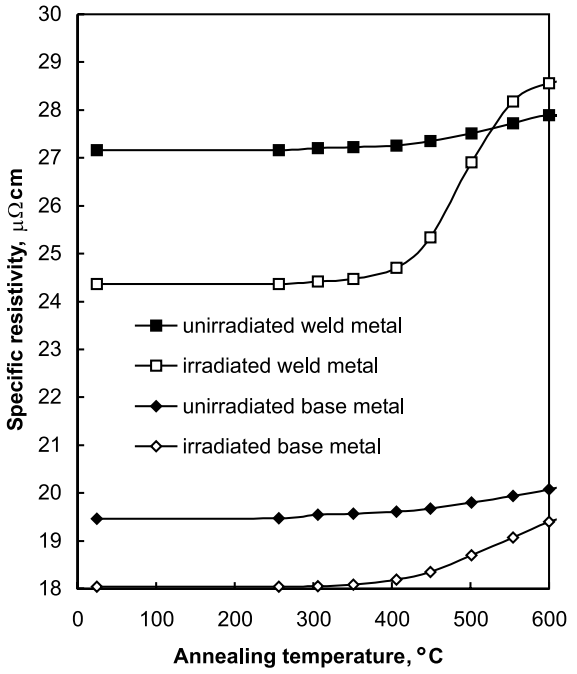

Fig. 3. Electrical resistivity change in liquid helium (−269 °C) as a function of annealing temperature for unirradiated and irradiated 15Kh2MFA base metal and Sv-10KhMFT weld metal. Irradiation: 4.1×10^{19} n/cm^2 at 265 °C, $E > 1$ MeV.

Table 2
Fitting results of the Mössbauer spectra

Sample	C	H (kOe)	IS (mm/s)	E_Q (mm/s)	Area (%)
Base metal, unirradiated	1	337.9	0.003	−0.006	56.4
	2	308.9	−0.008	−0.009	31.8
	3	280.4	−0.019	−0.012	7.1
	4	245.5	−0.100	−0.060	1.7
	5	133.3	0.081	0.078	1.7
	6	–	0.072	0.350	1.3
Base metal, irradiated	1	338.4	−0.003	−0.002	54.0
	2	308.9	−0.013	−0.009	37.6
	3	272.7	−0.022	−0.013	4.0
	5	131.6	0.091	−0.078	3.4
	6		0.084	0.243	1.0
Weld metal, unirradiated	1	337.0	0.004	−0.006	51.1
	2	309.9	0.001	−0.015	45.3
	3	273.2	0.020	−0.012	1.6
	5	129.6	0.097	−0.086	1.5
	6	–	0.083	0.348	0.5
Weld metal, irradiated	1	337.2	−0.001	−0.003	52.0
	2	309.6	0.002	−0.004	43.2
	3	273.2	−0.024	−0.013	1.8
	5	125.4	0.103	−0.087	2.3
	6	–	0.091	0.246	0.7

C = component, H = hyperfine magnetic field, IS = isomeric shift, E_Q = quadrupole splitting, area = relative intensity of the different components.

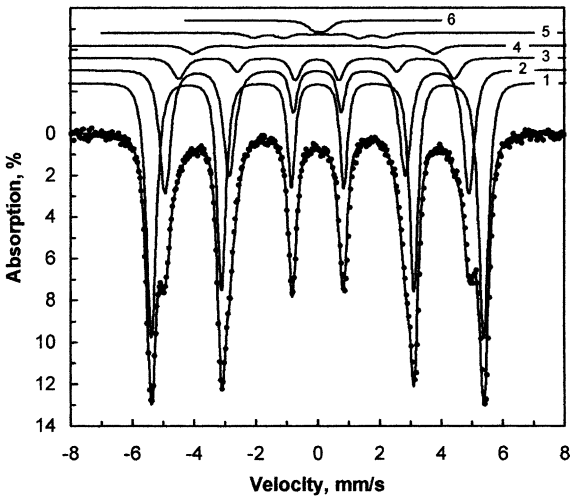

Fig. 4. Mössbauer spectrum of unirradiated 15Kh2MFA base metal.

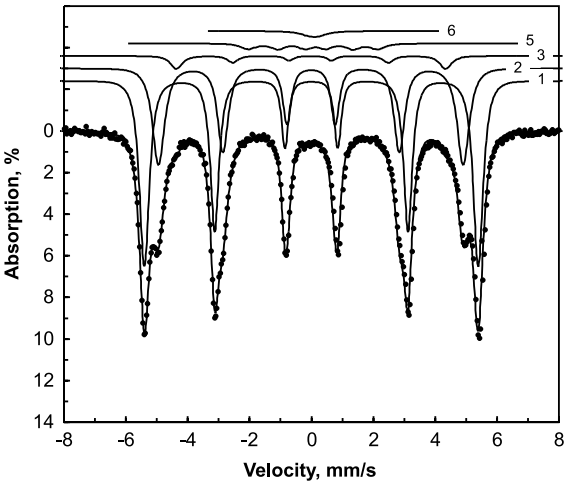

Fig. 5. Mössbauer spectrum of irradiated 15Kh2MFA base metal, irradiation: 4.1×10^{19} n/cm^2 at 265 °C, $E > 1$ MeV.

with their relatively large intensities, are rather clearly resolved in the outer side lines of the spectrum. However, components 4, 5 and 6 are not clearly resolved (Fig. 4). The relative intensities of components 4, 5 and 6 are approximately 1–2%, exceeding slightly the experimental error (0.5%).

The hyperfine structure of the spectrum of the irradiated base metal (Fig. 5) is similar to that of the unirradiated base metal. However, component 4 disappeared while components 5 and 6 remained in the spectrum. The hyperfine field (H) of component 5 and the quad-

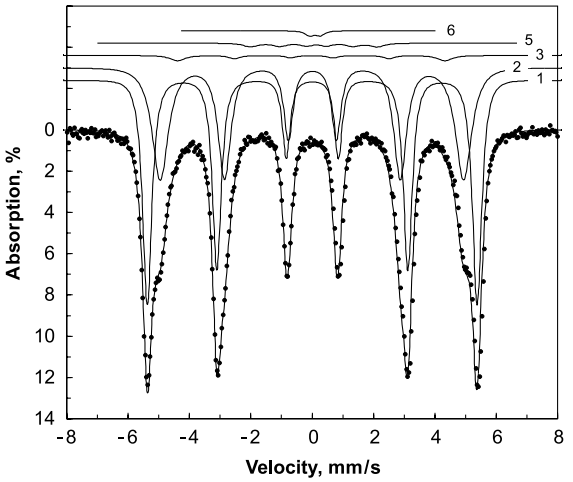

Fig. 6. Mössbauer spectrum of unirradiated Sv-10KhMFT weld metal.

rupole splitting (E_Q) of component 6 are clearly decreased. There are small changes in the integral intensities of the components: the intensities of components 2 and 5 are increased and the intensities of components 1 and 3 are decreased. The intensity of component 6 was not changed.

The hyperfine structure of the spectrum of the unirradiated weld metal consists of five components (Fig. 6). They correspond to components 1, 2, 3, 5 and 6 in the spectrum of the base metal, respectively (Fig. 4). Unlike components 1 and 2, the hyperfine magnetic field of components 3 and 5 became distinguishable when compared to the corresponding parameters of the base metal spectrum (Table 2). The integral intensity of component 2 was increased, which is consistent with the difference in the composition between the base and weld metals.

After irradiation, the hyperfine parameters of the spectrum of the weld metal were changed for components 5 and 6 (Fig. 7).

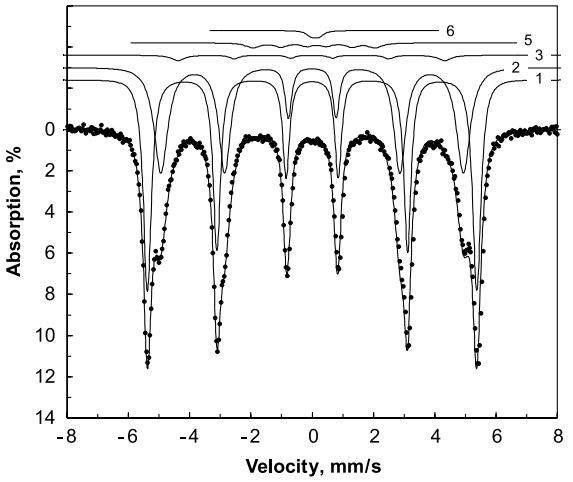

Fig. 7. Mössbauer spectrum of irradiated Sv-10KhMFT weld metal, irradiation: 4.1×10^{19} n/cm^2 at 265 °C, $E > 1$ MeV.

4. Discussion

4.1. Unirradiated state

The Mössbauer spectrum of the unirradiated base metal consists of six components (Fig. 4). According to the Mössbauer results of the substitutional iron alloys [10] and the Fe–C martensite [11], component 1 with its hyperfine field value ($H_1 \approx 337.9$ kOe) is attributed to iron atoms with no alloying elements as their nearest neighbours. Components 2 and 3 correspond to iron atoms with one and two alloying elements (C, Cr, Mo, V, Mn, Cu) as their nearest neighbours, respectively. Such components exist also in the Mössbauer spectra of the RPV steels studied in [12].

The slightly larger H value of component 1 as compared with the corresponding parameter of pure iron (333 kOe) was also noted in [12]. It can be consistent with the tendency to increase the hyperfine magnetic field at the nuclei of iron atoms due to alloying elements in the third and further coordination spheres [10]. The higher H value of component 1 can also be associated with the effect of Ni, the content of which is larger in the RPV steel studied here than in the steel studied in [12].

Component 4 with the hyperfine field, $H_4 \approx 245.5$ kOe, can be related to iron atoms in carbon clusters in the solid solution. Here clusters mean atomic distributions where the nearest interstitial sites in the vicinity of iron atoms are occupied by more than two atoms. The H value of component 4 is less than the corresponding parameter in the spectrum of the binary Fe–C alloy [11], and it is obviously associated with the effect of alloying elements such as Cr, Mn, V and Cu on the magnetic hyperfine interaction. It means that unlike the carbon clusters in Fe–C martensite, the clusters in the RPV steel may contain these alloying elements.

Components 5 and 6 (relative intensities 1.7% and 1.3%, respectively) belong to some precipitates containing iron and other alloying elements. Taking into account the parameter values of the hyperfine structure of the spectra of the alloyed carbide in the steel [13] and the values for isolated carbides in steels [14,15], it is possible to consider such precipitates as carbides (perhaps cementite) containing other substitutional atoms, which can be formed during the heat treatment of the base metal.

Hyperfine field of component 5 is smaller than that of cementite (208 kOe) in [16]. This may be the result of enrichment of the cementite by alloying elements [13].

As shown in [13,14,17], Mn and Cr reduce the hyperfine magnetic field at the nuclei of iron atoms, and at certain contents of Mn and Cr, hyperfine magnetic structure vanishes. Since the magnetic state of the cementite depends on concentration [13,14,17], and since the special iron carbides with Cr, Mo, W and V contribute to the Mössbauer spectrum as a singlet or a doublet [15], component 6 in the spectrum of the base metal is related to a paramagnetic carbide enriched by the alloying elements. More accurate interpretation of this component is rather difficult due to its insufficient resolution.

The line widths (full width at half maximum) of the carbide components 5 and 6 ($\Gamma_{1,6} \approx 0.572$ mm/s for component 5 and $\Gamma_{1,2} \approx 0.552$ mm/s for component 6) are larger than those of component 1 ($\Gamma_{1,6} \approx 0.373$ mm/s) related to iron atoms in the ferrite, which means an inhomogeneous distribution of alloying elements and an existence of iron atoms with different atomic surroundings in the carbide or the existence of other types of carbides.

The distribution of the alloying elements is not significantly different in the unirradiated weld metal which is evident from the hyperfine structure of the Mössbauer spectrum (Fig. 6). The disappearance of the cluster component 4 in the resonant spectrum is consistent with the small amount of carbon in the weld metal (0.04 wt%) as compared with that of the base metal (0.16 wt%). Moreover, the larger contents of Si, Mn and Cu, as well as the smaller Cr content in the weld metal than in the base metal cause changes in the short-range ordering in the substitutional system. That is exhibited by the increase of the relative amount of iron atoms with one alloying element in the first coordination sphere (Fig. 5, Table 2, component 2) and the decrease of the fraction of the iron atoms with two or more substitutional atoms as their nearest neighbours (Fig. 5, Table 2, component 3). The fraction of the precipitates was not significantly changed, which is evident from the integral intensity of the carbide components 5 and 6.

Thus, according to the Mössbauer measurements, in spite of the insufficient resolution of the components 4–6 in the spectra (Fig. 4) and independent of their interpretation, the atomic distribution in the unirradiated base metal (after tempering at 700 °C) and in the weld metal is not homogeneous and it is characterized by the existence of impurities, clusters and carbides.

Atomic redistribution during annealing of the unirradiated base and weld metals was examined by electrical resistivity, which is sensitive to the structural changes of steels and redistribution of impurity atoms. The slightly visible increase in the resistivity after heating at temperatures above 350–400 °C indicates an increase of electron scattering centers (Fig. 3), which can be caused by release of the impurity atoms from the quenching- and welding-induced defects and their redistribution in the solid solution. This result is not in agreement with the discussion of the study in [5] where the authors interpreted a slight permanent increase of the average positron lifetimes in 15Kh2MFA steels as a result of coarsening of larger vanadium carbides at the expense of smaller precipitates. However, in the case of only a change in the size of the precipitates, the resistivity should not be increased.

4.2. Irradiated state

Atomic distribution was changed in the base metal due to irradiation (4.1×10^{19} n/cm^2, $E > 1$ MeV, 265 °C). As it follows from the changes of the integral intensity of the Mössbauer spectrum components (Table 2) the absence of component 4 in the resonance spectra (Fig. 5) means that carbon clusters disappeared and transformed perhaps to alloyed cementite or special carbides. The decrease in the intensity of the component 3, which relates to iron atoms with carbon atoms or alloying elements in the first coordination sphere, and the increase of the fraction of the carbide component 5 confirms such description of atomic redistribution in the solid solution under irradiation, and also an increase in the amount of carbides.

The disappearance of the internal friction peak in the irradiated state (Fig. 2) is due to the trapping of carbon atoms in the irradiation-induced defects [18–20]. They are probably not vacancies, because of the irradiation temperature (265 °C), where vacancies are able to move freely and therefore to anneal out, e.g. by recombination with interstitials or by diffusion to sinks such as grain boundaries. Thus, there will be a balance between the production and the annealing of the vacancies during irradiation according to [5], where carbide formation was supposed to take place in the same type of RPV steel due to irradiation. This can also be the reason for the disappearance of the Snoek peak [21]. The other possible trapping defects can be irradiation-induced defects: interstitials, dislocations or vacancy clusters created in collision cascades.

The decrease in the relative area of the component 3 can be partially associated with the transition of carbon atoms from their interstitial sites due to capture by irradiation-induced defects and partially with the formation of carbides [12,15,19,22]. It could not be identified, if such alloying elements as Cr, Mn, Cu, etc. took part in the redistribution process in the base metal, from the results mentioned above due to the weak resolution of the spectral components and the close values of the parameters of hyperfine structure.

Neutron irradiation normally increases electrical resistivity due to the formation of point defects, i.e. vacancies and interstitials. The observed decrease in electrical resistivity (Fig. 3) can be due to the decrease in the dislocation density under irradiation and/or irradiation-induced precipitation. The decrease in the dislo-

cation density has been observed in TEM investigations of 15Kh2MFA steel where 1.2×10^{23} n/m^2 ($E > 1$ MeV) neutron dose decreased the dislocation density by an order of $1–2 \times 10^{14}$ l/m^2 [6]. The other main reason for the resistivity decrease may be irradiation-induced precipitates such as Cu- and P-rich precipitates. Brauer et al. [5] have proposed irradiation-induced $M_{23}C_6$-type carbide formation in a 15Kh2MFA steel, with an expected radius in the range of 0.63–4.5 nm. Also changes in the short-range atomic ordering due to irradiation can cause decrease of electrical resistivity during irradiation [23]. One reason for the decrease in the electrical resistivity can be the reduction of the scattering centers, such as interstitial atoms or other defects due to the irradiation as a result of the irradiation temperature (265 °C). On the contrary, in the case of 'freezing' of the vacancies after irradiation the resistivity should be increased.

The increase in electrical resistivity, occurring in the irradiated specimens at temperatures above 350 °C, may be due to release of impurities that were trapped in the irradiation-induced vacancy clusters. Also small coherent precipitates may have been formed. The irradiation-induced changes in the specific electrical resistivity values are not absolute because the irradiated and the unirradiated specimens were not the same. Also the results may have been affected by the inhomogeneity of the specimens, although the specimens were cut next to each other.

The formation of voids and microcavities in RPV steels during high-temperature irradiation was not confirmed in the positron annihilation or small angle X-ray scattering studies [24,25]. Moreover, since the Snoek peak did not reappear after annealing at 450 and 475 °C (1 h) (Fig. 2), carbon atoms were not released from their trapping sites during the recovery annealing, which would be possible if carbon atoms were captured by defects such as vacancy clusters, because the annealing temperature of microcavities is below 350 °C [25]. The constant value of the resistivity during annealing up to the temperature of 400 °C (Fig. 3) confirms the above interpretation of the behaviour of carbon atoms and defect structure.

The irradiation-induced dislocation loops created in the collision cascades during high-temperature irradiation can be most probable traps for carbon atoms due to the strong interaction between carbon atoms and dislocations. Binding energy between a dislocation and a carbon atom in iron is 0.75–0.85 eV [26]. On the other hand, the increase in the integral intensity of component 5 in the Mössbauer spectrum (Table 2) supports the assumption that the disappearance of the Snoek peak in Fig. 2 is due to the binding of carbon atoms in carbides during irradiation.

Mössbauer spectroscopy results reveal that there is no significant change in the atomic distribution in the solid solution of the irradiated weld metal as compared with that in the unirradiated state (Figs. 6 and 7). The small increase in the integral intensity of components 5 and 6 confirms the tendency to carbide formation during neutron irradiation. Diffusion of the alloying elements to cementite also takes place because the value of the hyperfine magnetic field was decreased.

It was not possible to point out that the increase in the electrical resistivity of the irradiated specimens during annealing in the temperature range of 400–500 °C is connected to the release of impurity atoms from the defects, or partial dissolution of the precipitates because the internal friction results do not confirm the reappearance of carbon atoms in the solid solution during the annealing in that temperature range.

The temperature range of recovery lies in the temper embrittlement temperature range (375–575 °C), where P, Si and Sb tend to segregate to grain boundaries and thus increase the ductile-to-brittle transition temperature. Temper embrittlement occurs most rapidly around 450–475 °C, which is the planned recovery annealing temperature range for the VVER-440 pressure vessel steels. Therefore, temper embrittlement should not be ignored while predicting the recovery annealing behaviour, although this steel has molybdenum as an alloying element, which is known to reduce the susceptibility to temper embrittlement phenomenon.

5. Conclusions

The following conclusions can be drawn from the measurements:

(1) Atomic distribution is not homogeneous in the base (15Kh2MFA steel) and weld metals (Sv-10KhMFT) studied.
(2) Neutron irradiation causes atomic redistribution in the base and weld metals. The matrix is depleted of interstitial atoms, probably due to the strong interaction between irradiation-induced dislocations and carbides. This is accompanied by a decrease in the electrical resistivity.
(3) Annealing of the unirradiated or irradiated base or weld metals does not change the electrical resistivity at temperatures below 400 °C. The increase in the electrical resistivity at temperatures above 400 °C may be caused by a release of impurity atoms from irradiation-induced defects or partial dissolution of irradiation-induced precipitates.
(4) The small amount of carbon in the base metal matrix and the matrix inhomogeneity make it difficult to study 15Kh2MFA steel using internal friction Snoek peak measurements. Also the very complicated carbide structure makes the interpretation of the results difficult. Thus, in future measurements of interactions between irradiation-induced defects

and interstitial atoms, i.e. carbon, nitrogen and oxygen, well-characterized model alloys should be used.

(5) The electrical resistivity measurements proved to be a sensitive method to measure recovery annealing temperature ranges. Both the base and the weld metal started to recover at temperatures above 350 °C. The main recovery took place in the temperature range of 400–550 °C. The interpretation of the electrical resistivity changes is difficult due to numerous factors. Thus, to understand the irradiation embrittlement and recovery annealing mechanisms, electrical resistivity measurements should be complemented by ATEM investigations.

(6) Mössbauer spectroscopy is an effective tool to study atomic environments of the iron isotope probe atoms. According to the measurements, there is some evidence of carbide precipitation under irradiation. The internal friction and the electrical resistivity measurements support this assumption. Because the interpretation of the Mössbauer spectra is difficult in complex steels, the carbide types or their composition could not be identified. In the future, more simple model alloys should be used to study these phenomena in RPV steels by using Mössbauer spectroscopy.

Acknowledgements

This research was a part of VTT RATU research programme. TES (Tekniikan edistämissäätiö, Finland) is especially acknowledged for supporting this investigation.

References

[1] R. Havel, Reactor pressure vessel embrittlement, International Atomic Energy Agency, IAEA-TECDOC-659, 1992.
[2] W.J. Pythian, C.A. English, J.T. Buswell, Proceedings of the 5th International Symposium on Environmental Degradation of Metals in Nuclear Power Systems–Water Reactors, Monterey, CA, USA, August 25–29, 1991, ANS, La Grange Park, 1992.
[3] B.A. Gurovich, E.A. Kuleshova, Yu.A. Nikolaev, Ya.I. Shtrombakh, J. Nucl. Mater. 246 (1997) 91.
[4] J. Böhmert, H.-W. Viehrig, A. Ulbricht, J. Nucl. Mater. 297 (2001) 251.
[5] G. Brauer, L. Liszkay, B. Molnar, R. Krause, Nucl. Eng. Des. 127 (1991) 47.
[6] J. Kocik, E. Keilová, J. Nucl. Mater. 172 (1990) 126.
[7] K. Törrönen, Microstructural parameters and yielding in a quenched and tempered Cr–Mo–V pressure vessel steel, Technical Research Centre of Finland, Report VTT-22, 1979.
[8] K. Ullakko, Aging of iron based martensites at low temperatures, Helsinki University of Technology, Laboratory of Engineering Materials, Report 3, 1992.
[9] A.S. Nowick, B.S. Berry, Anelastic Relaxations in Crystalline Solids, Academic Press, New York, 1972.
[10] G.K. Wertheim, V. Jaccarino, J.H. Wernick, D.N.E. Buchanan, Phys. Rev. Lett. 12 (1964) 24.
[11] J.M.R. Genin, P. Flinn, Trans. TMS-AIME 343 (1968) 1419.
[12] G. Brauer, W. Matz, Cs. Fetzer, Hyperfine Interact. 56 (1990) 1563.
[13] V.N. Gridnev, V.G. Gavriljuk, V.M. Nadutov, Phys. Met. Metall. 60 (1985) 590.
[14] G.P. Huffman, P.R. Errington, R.M. Fisher, Phys. Stat. Sol. (a) 22 (1967) 473.
[15] E. Kuzmann, E. Bene, L. Domonkos, Z. Hegedüs, S. Nagy, A.J. Vertes, J. Phys. 37 (1976) C6–409.
[16] M. Ron, H. Shechter, S. Niedzwicdz, J. Appl. Phys. 39 (1968) 265.
[17] P. Schaaf, S. Wiesen, U. Gonser, Acta Met. Mater. 40 (1992) 373.
[18] H. Wagenblast, A.C. Damask, J. Phys. Chem. Solids 23 (1962) 221.
[19] M.S. Wechler, K.L. Murty, Met. Trans. 20A (1989) 2637.
[20] J. Takahashi, T. Yamane, J. Nucl. Sci. Technol. 12 (1975) 634.
[21] J.T. Stanley, Conference on Diffusion in Body-Centered Cubic Metals, Gatlinburg, Tennessee, USA, September 16–18, 1964, American Society for Metals, Metals Park, OH, 1965.
[22] G. Brauer, R. Krause, A. Polity, Annealing studies of neutron irradiated reactor pressure vessel steels by positron annihilation, Zentralinstitut für Kernforschung Rossendorf, Report Zfk-647, 1988.
[23] K. Nakata, S. Takamura, I. Masaoka, J. Nucl. Mater. 131 (1985) 53.
[24] K. Ghazi-Wakili, U. Zimmermann, J. Brunner, P. Tipping, W.B. Waeber, F. Heinrich, Phys. Stat. Sol. (a) 102 (1987) 153.
[25] C. Lopes Gil, A.P. De Lima, N. Ayres De Campos, J.V. Fernandes, G. Kögel, P. Sperr, W. Triftshäuser, D. Pachur, J. Nucl. Mater. 161 (1989) 1.
[26] H. Hänninen, Y. Yagodzinskyy, O. Tarasenko, H.-P. Seifert, U, Ehrnsten and P. Aaltonen, in: Proceedings of the 10th International Conference on Environmental Degradation of Materials in Nuclear Power Systems–Water Reactors, Lake Tahoe, NV, USA, September 5–9, Nace, in press.